Title

T2* placental MRI in pregnancies complicated with fetal congenital heart disease

Authors

Johannes K Steinweg [1]; Grace Tin Yan Hui [3]; Maximilian Pietsch[3,4], Alison Ho [3]; Milou PM van Poppel [1]; David Lloyd [1,2]; Kathleen Colford [3]; John M Simpson [1,2], Reza Razavi [1,2], Kuberan Pushparajah [1,2]; Mary Rutherford [3], Jana Hutter [3,4]

Affiliations

1. Department of Cardiovascular Imaging, School of Biomedical Engineering & Imaging Science, King's College London, London, United Kingdom
2. Department of Congenital Heart Disease, Evelina Children's Hospital, London, United Kingdom
3. Centre for the Developing Brain, King's College London, London, United Kingdom
4. Department of Biomedical Engineering, School of Biomedical Engineering & Imaging Science, King's College London, London, United Kingdom

Corresponding author

johannes.steinweg@kcl.ac.uk
Johannes K Steinweg
Department of Cardiovascular Imaging
Wellcome/EPSRC Centre for Medical Engineering
School of Biomedical Engineering & Imaging Sciences
King's College London
3rd Floor Lambeth Wing
St. Thomas' Hospital
Westminster Bridge Road
London SE1 7EH
United Kingdom

Abstract

Background

Congenital heart disease (CHD) is one of the most important and common group of congenital malformations in humans. Concurrent development and close functional links between the fetal heart and placenta emphasise the importance of understanding placental function and its influence in pregnancy outcomes. The aim of this study was to evaluate placental oxygenation by relaxometry (T2*) to assess differences in placental phenotype and function in CHD.

Methods

In this prospective cross-sectional observational study, 69 women with a fetus affected with CHD and 37 controls, whole placental T2* was acquired using a 1.5-Tesla MRI scanner. Gaussian Process Regression was used to assess differences in placental phenotype in CHD cohorts compared to our controls.

Results

Placental T2* maps demonstrated significant differences in CHD compared to controls at equivalent gestational age. Mean T2* values over the entire placental volume were lowest compared to predicted normal in right sided obstructive lesions (RSOL) (Z-Score 2.30). This cohort also showed highest lacunarity indices (Z-score -1.7), as a marker of lobule size. Distribution patterns of T2* values over the entire placental volume were positively skewed in RSOL (Z-score -4.69) and suspected, not confirmed coarctation of the aorta (CoA-) (Z-score -3.83). Deviations were also reflected in positive kurtosis in RSOL (Z-score -3.47) and CoA- (Z-score -2.86).

Conclusion

Placental structure and function appear to deviate from normal development in pregnancies with fetal CHD. Specific patterns of altered placental function assessed by T2* deliver crucial complementary information to antenatal assessments in the presence of fetal CHD.

Keywords

Congenital Heart disease (CHD), Placenta, Magnetic resonance imaging (MRI), T2* Mapping, Gaussian Process Regression (GPR), Machine learning

Introduction

Congenital heart disease (CHD) is a common group of congenital malformations with a prevalence of up to 1% of all live births, a leading cause of neonatal and infant death and a global burden in child health [1,2]. Underlying aetiology is considered multifactorial combining genetic, epigenetic and environmental causes [3–5]. Recently, placental vascular malperfusion has been reported at pathological examination in association with CHD [6,7] and it has been postulated that this may contribute to the neurodevelopmental abnormalities observed in children with CHD [8].

The placenta is the only connection between the fetal and maternal circulation. It plays a pivotal role in fetal development due to its responsibility for all fetomaternal exchange, including oxygen, carbon dioxide and nutrients, and essential immunological and homeostatic functions. The placenta and fetal heart develop concurrently and share similar developmental pathways – amplifying its unique role and vulnerability to disturbances especially in the presence of fetal CHD [9,10]. A sophisticated in vivo assessment of placental structure and function may inform understanding of complex antenatal pathophysiology in pregnancies with fetal CHD and help to identify fetuses at greater risk of adverse long term neurodevelopmental outcomes.

A common MR contrast mechanism employed to study tissue oxygen concentration is produced by the blood oxygen level dependency (BOLD) effect, exploited in quantitative T2 relaxometry (T2*). The parametric properties of deoxyhaemoglobin allow for a faster T2* decay than its oxygenated counterpart [11,12]. Widely used in functional brain MRI, it has also recently found application in placental MRI, allowing in-vivo insights into the tissue properties without the use of exogenous contrast agents [13–15].

Previous studies in humans have shown a linear negative correlation of placental mean T2* values over gestational age (GA) and found it to be predictive for low birth weight [15,16]. An increase in placental mean T2* was previously reported in response to maternal oxygen administration [17,18]. Decreased mean T2* values can be induced by vasoconstrictive agents in animal models and have been demonstrated in pregnancies with fetal growth restriction in both animals and humans [19–21]. Reduced whole placental mean T2* values for GA were recently also associated with preeclampsia [22].

Mean T2* value calculated over the placental parenchyma, either assessed in selected slices or the entire placental volume have been used for quantification in previous

studies. However, novel advances extend this to include spatial analysis using histograms and texture-based measurements, first shown in rhesus monkeys [23,24]. This study aimed to evaluate whether CHD is associated with altered placental phenotype and function, including signs of lower oxygenation and altered tissue morphology, as estimated by high-resolution whole placental MR relaxometry (T2*) and to establish methods to evaluate deviations from the expected values over GA.

Methods

In this prospective cross-sectional observational study, we recruited pregnant women carrying a fetus diagnosed with congenital heart disease (CHD) from a tertiary fetal cardiology service for CHD (St Thomas' Hospital, London, UK) alongside a control group of women with uncomplicated pregnancies during the second and third trimester. Inclusion criteria for both cohorts were singleton pregnancy, maternal age over 18 years and ability to consent in English language. Exclusion criteria for both cohorts were multiple pregnancies, major maternal health issues, any treatment for hypertension at time of scan as well as contraindications for MRI such as metallic implants and claustrophobia. Exclusion criteria for controls also included diagnosis of fetal or intrauterine growth restriction (FGR/IUGR) and low birth weight (SGA), signs of preeclampsia or (gestational) diabetes at time of scan.

Prospectively specified data collection included demographic characteristics and maternal pregnancy data at time of scan, as well as delivery notes and neonatal outcomes. Maternal data included age and BMI at scan, parity, gravida, medical history of smoking, (gestational) diabetes, hypertension, preeclampsia, HELLP syndrome, thyroid disease and anxiety or depression as noted at time of scan and in their delivery notes. Neonatal data included fetal and neonatal cardiac diagnosis, sex, GA at scan and birth, birth weight, 5 min APGAR, neonatal outcome, genetic testing, suspicion of genetic abnormality and place of birth as noted on the delivery or (cardiology) discharge notes.

Centiles and standard scores for birth weight were calculated following the INTERGROWTH-21st project [25]. SGA was defined as birthweight less than 10th centile in keeping with common clinical practice. Our CHD cohort was classified into 7 groups based on the main antenatal diagnosis (Figure 1, Table 1). We divided our cohort into left sided obstructive lesions, namely hypoplastic left heart syndrome (HLHS) and coarctation of the aorta (CoA), right-sided obstructive lesions (RSOL) defined as structural or functional obstruction of the right ventricular outflow tract, disorders of mixing (e.g., transposition of the great arteries (TGA)), suspected vascular rings (VR) and other major lesions comprising of common arterial trunk (CAT), partial anomalous pulmonary venous drainage (PAPVD) and cardiac rhabdomyomas (CR). The group of suspected CoA was further divided by those with postnatal confirmation requiring surgery within the neonatal period (CoA+) and without postnatal CoA during follow up (CoA-). All our infants are therefore followed up by our team at least until 1 year of age.

Ethics:

This study was approved by London Research Ethics Committees of the Health Research Authority (HRA) of the Department of Health in the United Kingdom, "Quantification of fetal brain growth and development using MRI" (REC: 07/H0707/105), "Fetal Imaging with Maternal Oxygen" (REC: 17/LO/0282) and "iFIND-2. Further Imaging" (REC: 14/LO/1806). Controls were also included from the "Placenta Imaging Project" (REC: 16/LO/1573).

MRI Acquisition:

All women were scanned using a clinical 1.5-Tesla Philips Achieva MRI with a 28-channel torso coil under clinical monitoring and medical cover during the entire scan. All mothers carrying a fetus with CHD were scanned in left lateral tilt. A multi-echo gradient echo sequence covering the entire uterus in coronal orientation was acquired with a resolution of 2.5mm isotropic, FOV=360x360, 50-88 slices, no SENSE, no half-scan, TR=14s, TE=11.376ms / 57.313ms / 103.249ms / 149.186ms / 195.122ms, free breathing, TA=1min.

MRI data processing:

T2* maps were calculated using an in-house monoexponential fitting in MATLAB (The MathWorks Inc, USA). The whole placenta was manually segmented by experienced observers (JKS, GH, AH, JH) using ITK-SNAP [26], with exactly matched instructions to segment the placenta conservatively, avoiding inclusion of both amniotic fluid and maternal vasculature. Reproducibility of manual segmentations between observers was assessed using the Sørensen–Dice coefficient [27].

The masks were automatically refined by excluding non-physiological values. Mean T2*, skewness, kurtosis and lacunarity values were obtained using a purpose-build python script [13,28]. Lacunarity values thereby reflect the spatial distribution of gaps of a specific size within lobules [29] and a box-size matched to typical placental lobule size.

To estimate placental development over GA we used Gaussian Process Regression (GPR), a Bayesian non-parametric regression [30]. Clinical cohorts are inherently heterogenous necessitating an estimation of uncertainty of probable distributions. Accounting for this and a covariance between the data points GPR provides normative group mean function, allowing point estimates and predictive confidence for each observation. This allows the calculation of standard (Z-) scores for all measured test data points, describing the distance to expected value following the normative group mean function [31].

The control cohort was split into training and test data (0.7 to 0.3 ratio) and the test subjects were used to train the model. The kernel function used was an additive combination of Constant function, Radial Basis Functions and Noise kernel. The data was scaled pre-training. Predictive posterior distributions were obtained for mean T2*, lacunarity, skewness and kurtosis separately. Z-scores for the observed values were derived for all CHD cohorts by estimation of mean deviation and median deviation from GPR predicted value normalised by the prediction uncertainty.

For comparison of clinical parameters controls were restricted to GA at scan between 28 and 37 weeks to match GA for CHD cohort, categorical variables were compared using Fisher's exact test, continuous variables were evaluated for normality by Shapiro compared using Independent T-test (normal distribution), 2-tailed Mann-Whitney U test (non-normal distribution). Dependence of results from clinical parameters was evaluated by coefficient of determination. All statistical analysis and visualisation were performed using SPSS Statistics v27 (IBM) and Jupyter Notebook, python3.

Results

Maternal and neonatal demographics are demonstrated in Table 1. Overall, 119 participants were enrolled in this study. Eight subjects from our CHD cohort were excluded: for twin pregnancy (n=1), insufficient scan data (n=3) and insufficient outcome data at time of analysis (n=4). Five controls were excluded for small for GA at birth (n=3) and insufficient scan data (n=2). In total 69 women with pregnancies with fetal diagnosis of CHD and 37 women with uncomplicated pregnancies were included in the analysis (Figure 1). The median GA at scan was 31.3 weeks (IQR 2.21) and 31.2 weeks (IQR 8.11) respectively. Results of genetic testing from antenatal invasive procedures or postnatal blood sample using at least array comparative genomic hybridization (aCGH) were available for 46 (67%) subjects in our CHD cohort. 5/46 identified an abnormal result (two with Chr 2q31 deletion, one with a Chr 9 deletion and gene copy number on Chr 2, one with TSC1 gene mutation, and one with mosaic Monosomy X). All remaining patients caused no phenotypic suspicion for a genetic abnormality after birth.

Seven newborns with CHD from our cohort died due to necrotising enterocolitis (1), hypoxic ischemic encephalopathy (1), congenital diaphragmatic hernia (1) and cardiac collapse or palliation (4). The CHD cohort had a higher incidence of low APGAR score (<7) at 5 minutes ($p=0.024$) compared to our control cohort. GA at birth ($p<0.001$) and birth weight ($p<0.001$) and birth head circumference ($p=0.005$) were significantly lower in the CHD cohort, whose mothers were also younger ($p=0.017$). None of the other clinical collected parameters achieved clinical significance.

We have reviewed medical records at time of scan and delivery. Our CHD cohort included three women diagnosed with preeclampsia (4.3%). Two needed delivery at 32 weeks of gestation, one for severe HELLP and one for uncontrollable hypertension. One woman delivered after induction early term at 37 weeks of GA.

In our CHD cohort 18 (26%) newborns were born <10^{th} birth weight centile (SGA), 25 (36%) newborns were born with low head circumference (HC) <10^{th} centile, 13 newborns (19%) were SGA and had low HC. Only one of these 13, would be defined as growth restricted following the consensus-based definition in the newborn by Beune et al. [32].

Placental histology was available in 12 pregnancies complicated by fetal CHD on special clinical request mostly due to maternal pyrexia during delivery (Supplemental Table 1). From the two placentas demonstrating signs of maternal vascular malperfusion (MVM), one placenta showed also acute subchorionitis and maternal

inflammatory response (MIR) in keeping with ascending intra-uterine infection showing infarcts of variable age, but no thrombi. The other placenta was from a patient diagnosed with severe preeclampsia and HELLP syndrome leading to early delivery. Placental histology was also available for 15 control subjects as part of other study protocols (Supplemental Table 1).

Qualitative assessments

Placental T2* maps in our cohort of RSOL showed most marked differences compared to age-matched controls as depicted in mid-parenchymal slices (Figure 2). Specifically, short T2* values were noted in the entire placenta with additional and faster decay from the centre to the periphery of the lobules. Furthermore, increased heterogeneity could be observed in RSOL. Our cohorts of left sided obstructive lesions, disorders of mixing and other lesions appeared only moderately different to controls at similar GA (Figure 2). Overall, our CHD cohort appeared to have generally lower signal intensity throughout the placenta, advanced lobularity and higher granularity within the lobules at a given GA compared to our control cohort.

Quantitative assessments

Interobserver variability of manually segmented placental masks showed good correlation in 10 randomly selected with a Sørensen–Dice coefficient of 0.87. Quantitative results from the control cohort illustrate decay in mean T2* with increasing GA, in keeping with previous literature [15,29]. Lacunarity, kurtosis and skewness tend to increase over GA in all our cohorts as previously shown in controls [28]. The obtained posterior mean of the Gaussian process is given for all quantitative values in Figure 3.

Mean T2* values over the entire placental volume were lowest compared to predicted normal in RSOL (Z-Score 2.30) and our cohort with other major lesions [CAT, PAPVD, CR] (Z-Score 2.31). Our CoA- cohort had a larger deviation from expected values (Z-Score 1.39) than CoA+ (Z-score 0.24). Mean T2* values for HLHS (Z-score 0.63), VR (0.09) and TGA (Z-score -0.11) were within one standard deviation (SD) from expected results.

RSOL (Z-score -1.7), our group of other major lesions (Z-score -1.26) and CoA- (Z-score -1.02) showed significantly higher lacunarity compared to expected results at GA equivalent. HLHS (Z-score -0.18), TGA (Z-score -0.01) and suspected VR (Z-score 0.06) were similar to expected controls. CoA+ showed slightly lower lacunarity (Z-score 0.26).

Distribution of T2* values over the entire placental volume was positively skewed in RSOL (Z-score -4.69) and CoA- (Z-score -3.83), followed by our group of other major lesions (Z-score -1.75) and HLHS (Z-score -1.12). Suspected VR (Z-score -0.8), CoA+ (Z-score -0.66) distributions were positively skewed within one SD. Our TGA cohort was closest to expected skewness (Z-score 0.02).

We found positive kurtosis of distribution most significantly in RSOL with highest mean deviation (Z-score -3.47), followed by CoA- (Z-score -2.86) and our group of other major lesions (Z-score -1.97). HLHS and CoA+ showed positive kurtosis with almost one SD from expected results (Z-Scores -0.98), while suspected VR (Z-score -0.73) and TGA (Z-Score -0.27) showed similar kurtosis of distribution compared to our control cohort.

All placentas (19/69, 28%) with individual z-scores > ± 3 for any of calculated results were individually reviewed for correlation with clinical confounders, while we found MVM in two placentas and SGA complicating one pregnancy, overall numbers did not reach statistical significance.

Mean and median deviation form GP (Z-score) for all cohorts and measured values are listed in Table 2. Individual heterogeneity is demonstrated in histograms of occurrence fraction of T2* values in all voxels within the individual placenta from all participants in Figure 4. These histograms are color-coded by results of genetic testing in Supplemental Figure 1.

Maternal BMI at scan did not have an effect on mean T2* values ($R^2 = 0.004$). Maternal lie supine or left lateral, 30 and 7 scans respectively, had no significant effect on mean T2* values in our control group ($p = 0.44$). Placental position dichotomised in mostly anterior or posterior was also not associated with mean T2* values ($p = 0.98$). There was no linear correlation with mean T2* Z-scores at scan and weight ($R^2 = 0.13$) or head circumference at birth ($R^2 = 0.11$).

Discussion

In this study we have shown for the first time a comprehensive approach to placental tissue characterisation in CHD. Using T2 relaxometry (T2*) and Gaussian Process Regression (GPR) we were able to provide standard deviations for a range of placental metrics across various CHD groups from predicted values derived by our model trained on a control group. Mean T2* values over the entire placenta may not represent regional differences adequately and can lead to misinterpretation of imaging findings. Therefore, we also used histograms and evaluated skewness and kurtosis to show specific pattern of distribution depending on CHD subtype, which in turn may represent pathophysiological substrates.

Requiring minimal acquisition time (<1min) and minor modification to clinical scan protocols, these baseline placental assessments have been included into all our clinical fetal MRI scans.

While mean T2* deviation for RSOL (Z-score 2.30) is comparable with our group of other cardiovascular lesions (Z-score 2.31), the latter shows much less deviation from calculated normal distribution as described in skewness and kurtosis (Z-scores -1.75 and -1.97, respectively). Strikingly, right-sided obstructive lesions (RSOL) show highest deviation from expected normal distribution represented in skewness (Z-score -4.69) and kurtosis (Z-score -3.47).

Our findings of abnormal placental imaging appear CHD lesions specific. One might speculate that common intrinsic developmental pathways of placenta and fetal heart may play a larger role, warranting further investigations towards understanding the pathophysiology. Future investigations in conjunction with assessments of fetal circulation in the presence of CHD, a flourishing field in both ultrasound and MRI research [33,34], may allow a more detailed interpretation of our results.

Given the severe implications after birth, the cohort of HLHS appears to have surprisingly limited deviations from control in placental structure and function. This suggests less co-dependence between the development and or antenatal effects of this anomaly and the development and function of the placenta also requiring further research.

Our findings are in keeping with data from a very large Danish cohort from Matthiesen et al. also depicting an association of RSOL, but not left outflow tract obstructions including HLHS, aortic valve stenosis, and coarctation of the aorta, with lower placental weight [35]. Moreover Llurba et al. have suggested an imbalance in maternal and fetal

angiogenic factors may contribute to CHD and placental dysfunction most marked in cohorts other than left sided lesions [36].

Fetuses with antenatal suspicion of CoA without confirmation after birth (CoA-) were purposely not classified as controls in the design of this study. Firstly, presentation of CoA may present several weeks (up to a year) after closure of the arterial duct [37]. None of the infants included here showed signs of coarctation at the time of manuscript preparation. Secondly, there is a growing evidence that the observed ventricular asymmetry is a feature of abnormal loading conditions leading to abnormal myocardial deformation in fetuses with suspected coarctation [38]. In turn our CoA cohort spreads relatively widely through the range of values provided by our placental assessments (Supplemental Figure 2), which may reflect the wide clinical spectrum of CoA+ observed after birth, but also may indicate previously underexplored CHD entities some of which do not require an extensive surgical arch repair within the first year of life.

Studies of placental dysfunction and vascular malperfusion have shown altered baseline conditions on assessment with T2 relaxometry accounting for a higher relative response to maternal hyperoxygenation [15]. In our study we show similar altered placental baseline conditions in case of fetal CHD. This is a critical insight to understand the reported effects of short term maternal hyperoxygenation in CHD, which are being explored to improve fetal oxygenation in CHD [39].

Altered placental baseline functions are of particular importance to understand the complex intertwined fetomaternal environment in CHD and will also be essential to understand further approaches on antenatal intervention such as maternal hyperoxygenation [40].

Furthermore, structural assessments based on T2-weighted, and more recently also T1 imaging, depict changes over GA encompassing advanced lobulation with varied lobule sizes, higher granularity, and substantial areas of low-signal intensity and an increasing microstructural heterogeneity [41]. These changes are pronounced in FGR or PE compared to healthy controls [22,42]. Although we did not report weighted MR imaging in this study, observations from our T2* maps of increasing lacunarity over GA is in keeping with the literature for our control and CHD cohort. Moreover, our CHD cohorts also present higher lacunarity compared to healthy controls, most pronounced in RSOL (Z-score -1.70).

As previously reported factors such as maternal age, BMI, fetal sex, parity, mode of delivery and placental location were not correlated with T2* once corrected for GA [28].

Limitations of this study

Although we are based at a major referral centre for congenital heart disease in the UK, this was a single centre study, with some patients delivering outside of our hospital, having been referred for antenatal imaging. Our CHD groups are of moderate sample size and may influence statistical significance.

Our placental scan protocol consistent of one single timepoint, therefore temporal variance in placental T2* measurements, as recently suggested by other groups, might not be accounted for in our data [43]. Recent literature describes also the possible influence of maternal or placental position on T2* signals in higher field MRI [44]. While we have scanned all our CHD patients in left lateral position, controls were also scanned supine, resulting in higher statistical variance, 371.6 vs 776.5 respectively, but not reaching statistical significance.

While in-utero MRI provides an excellent opportunity to provide early, in-vivo evidence for specific placental phenotypes associated with CHD and hence a window of observation into the intertwined relation between developing heart and placenta, it cannot directly answer the question on causality and order of events.

Despite recent attempts to standardize definitions for FGR/IUGR, there is currently no universal definition, which would include fetuses with congenital malformations such as CHD [45]. Furthermore, the recent consensus-based definition of growth restriction on the newborn excludes congenital and chromosomal abnormalities specifically, although stating it may be applicable for this group due to the lack of any other option [32]. Previous literature, including a large population of 924,422 cohorts with over 5500 CHD cases from Denmark also suggests an association of some CHD subtypes with lower birth weight and head circumference [46]. Therefore, we did not exclude any participants in our CHD cohort solely due diagnosis for FGR/IUGR or SGA.

Placental histopathology results were only available in 25% of all our assessments and in CHD patients only with a specific clinical question at time of birth, such as maternal pyrexia. Statistical analysis of features of MVM or fetal vascular malperfusion (FVM) or Chorioamnionitis could therefore not be included. Similarly, only two placentas showed infarcts in histopathology. These could be identified on the in-vivo imaging but did not significantly alter the observed whole placental mean T2* results and have therefore not been factored in the statistical analysis. Previous literature from postnatal placental histopathology describe increased findings of FVM and MVM in the presence of preeclampsia as well as CHD supporting the hypothesis of similar etiopathogenetic factors contributing to the development of placental malformation and CHD [6].

While T2* values are an indicator of oxygen concentration, direct measurement was not possible in our setting. Oxygen-haemoglobin dissociation curves derived from MRI in animal models might be available for future studies to allow close estimation of actual oxygen content in the fetoplacental circulation [47,48].

Including only five pregnancies with confirmed fetal chromosomal abnormalities in our cohort did not allow for further statistical analysis of potential associations. This study did not include volumetric assessments of the placenta given echo planar imaging is associated with geometric distortions.

Future studies applied to CHD cohorts with more complex and time-consuming scan protocols, including diffusion-weighted imaging or texture analysis using T1 and T2 weighted methods, may allow modelling of fetal and maternal peculiarities in circulation and disentangle tissue characteristics and flow pathophysiology, as recently in CHD cohorts [41,49–51]. Slator et al. have recently published a study with a focused extensive research protocol on the microenvironments within the placenta depicting heterogenous compartments from maternal and fetal side [52]. Using Velocity-Selective Arterial Spin Labelled MRI Zun et al. also reported that global placental perfusion significantly decreased and regional variation of placental perfusion significantly increased over GA in fetuses with CHD [53,54].

Conclusion

This study describes in vivo differences in placental tissue phenotypes in healthy controls and fetuses with antenatal diagnosis of congenital heart disease based on T2 relaxometry. Using machine learning we depict unique features of T2* value distribution and their standard score from our normal cohort for a wide range of major cardiac lesions, providing information on placental dysfunction complementary in the antenatal assessment of CHD.

Acknowledgements

The authors acknowledge all clinical and scanning team involved in these projects and we are immensely grateful to the patients and volunteers recruited for this project.

Funding

This work was supported by the UKRI Future Leaders Fellowship [MR/T018119/1], the Wellcome/EPSRC Centre for Medical Engineering [WT 203148/Z/16/Z], the Wellcome Trust IEH Award 102431 (iFIND project), the NIH Human Placenta Project grant 1U01HD087202-01 (Placenta Imaging Project (PIP)), the Wellcome Trust Sir Henry Wellcome Fellowship [201374/Z/16/Z] and by the National Institute for Health Research (NIHR) Biomedical Research Centre based at Guy's and St Thomas' NHS Foundation Trust and King's College London. The views expressed are those of the authors and not necessarily those of the NHS, the NIHR or the Department of Health.

Declaration of competing interests

The authors declare that they have no competing interest.

Keywords

Congenital Heart disease (CHD), Placenta, Magnetic resonance imaging (MRI), T2* Mapping, Gaussian Process Regression (GPR), Bayesian non-parametric regression, Machine learning

References

[1] T. van der Bom, A.C. Zomer, A.H. Zwinderman, F.J. Meijboom, B.J. Bouma, B.J.M. Mulder, The changing epidemiology of congenital heart disease, Nature Reviews Cardiology. 8 (2011) 50–60. https://doi.org/10.1038/nrcardio.2010.166.

[2] M.S. Zimmerman, A.G.C. Smith, C.A. Sable, M.M. Echko, L.B. Wilner, H.E. Olsen, H.T. Atalay, A. Awasthi, Z.A. Bhutta, J.L. Boucher, F. Castro, P.A. Cortesi, M. Dubey, F. Fischer, S. Hamidi, S.I. Hay, C.L. Hoang, C. Hugo-Hamman, K.J. Jenkins, A. Kar, I.A. Khalil, R.K. Kumar, G.F. Kwan, D.T. Mengistu, A.H. Mokdad, M. Naghavi, L. Negesa, I. Negoi, R.I. Negoi, C.T. Nguyen, H.L.T. Nguyen, L.H. Nguyen, S.H. Nguyen, T.H. Nguyen, M.R. Nixon, J.J. Noubiap, S. Patel, E.K. Peprah, R.C. Reiner, G.A. Roth, M.-H. Temsah, M.R. Tovani-Palone, J.A. Towbin, B.X. Tran, T.T. Tran, N.T. Truong, T. Vos, K. Vosoughi, R.G. Weintraub, K.G. Weldegwergs, Z. Zaidi, B. Zheleva, L. Zuhlke, C.J.L. Murray, G.R. Martin, N.J. Kassebaum, Global, regional, and national burden of congenital heart disease, 1990–2017: a systematic analysis for the Global Burden of Disease Study 2017, The Lancet Child & Adolescent Health. 4 (2020) 185–200. https://doi.org/10.1016/S2352-4642(19)30402-X.

[3] D.K. Jarrell, M.L. Lennon, J.G. Jacot, Epigenetics and Mechanobiology in Heart Development and Congenital Heart Disease, Diseases. 7 (2019) 52. https://doi.org/10.3390/diseases7030052.

[4] Russell Mark W., Chung Wendy K., Kaltman Jonathan R., Miller Thomas A., Advances in the Understanding of the Genetic Determinants of Congenital Heart Disease and Their Impact on Clinical Outcomes, Journal of the American Heart Association. 7 (2018) e006906. https://doi.org/10.1161/JAHA.117.006906.

[5] S. Zaidi, M. Choi, H. Wakimoto, L. Ma, J. Jiang, J.D. Overton, A. Romano-Adesman, R.D. Bjornson, R.E. Breitbart, K.K. Brown, N.J. Carriero, Y.H. Cheung, J. Deanfield, S. DePalma, K.A. Fakhro, J. Glessner, H. Hakonarson, M.J. Italia, J.R. Kaltman, J. Kaski, R. Kim, J.K. Kline, T. Lee, J. Leipzig, A. Lopez, S.M. Mane, L.E. Mitchell, J.W. Newburger, M. Parfenov, I. Pe'er, G. Porter, A.E. Roberts, R. Sachidanandam, S.J. Sanders, H.S. Seiden, M.W. State, S. Subramanian, I.R. Tikhonova, W. Wang, D. Warburton, P.S. White, I.A. Williams, H. Zhao, J.G. Seidman, M. Brueckner, W.K. Chung, B.D. Gelb, E. Goldmuntz, C.E. Seidman, R.P. Lifton, De novo mutations in histone-modifying genes in congenital heart disease, Nature. 498 (2013) 220–223. https://doi.org/10.1038/nature12141.

[6] H. Miremberg, L. Gindes, L. Schreiber, A.R. Sternfeld, J. Bar, M. Kovo, The association between severe fetal congenital heart defects and placental vascular malperfusion lesions, Prenatal Diagnosis. 39 (2019) 962–967. https://doi.org/10.1002/pd.5515.

[7] J. Binder, S. Carta, J.S. Carvalho, E. Kalafat, A. Khalil, B. Thilaganathan, Evidence for uteroplacental malperfusion in fetuses with major congenital heart defects, PLOS ONE. 15 (2020) e0226741. https://doi.org/10.1371/journal.pone.0226741.

[8] S.D. Schlatterer, J. Murnick, M. Jacobs, L. White, M.T. Donofrio, C. Limperopoulos, Placental Pathology and Neuroimaging Correlates in Neonates with Congenital Heart Disease, Sci Rep. 9 (2019). https://doi.org/10.1038/s41598-019-40894-y.

[9] G.J. Burton, E. Jauniaux, Development of the Human Placenta and Fetal Heart: Synergic or Independent?, Front. Physiol. 9 (2018). https://doi.org/10.3389/fphys.2018.00373.

[10] J.A. Courtney, J.F. Cnota, H.N. Jones, The Role of Abnormal Placentation in Congenital Heart Disease; Cause, Correlate, or Consequence?, Frontiers in Physiology. 9 (2018) 1045. https://doi.org/10.3389/fphys.2018.01045.

[11] L. Pauling, C.D. Coryell, The Magnetic Properties and Structure of Hemoglobin, Oxyhemoglobin and Carbonmonoxyhemoglobin, Proceedings of the National Academy of Sciences. 22 (1936) 210–216. https://doi.org/10.1073/pnas.22.4.210.

[12] S. Ogawa, T.-M. Lee, A.S. Nayak, P. Glynn, Oxygenation-sensitive contrast in magnetic resonance image of rodent brain at high magnetic fields, Magnetic Resonance in Medicine. 14 (1990) 68–78. https://doi.org/10.1002/mrm.1910140108.

[13] J. Hutter, P.J. Slator, L. Jackson, A.D.S. Gomes, A. Ho, L. Story, J. O'Muircheartaigh, R.P.A.G. Teixeira, L.C. Chappell, D.C. Alexander, M.A. Rutherford, J. V. Hajnal, Multi-modal functional MRI to explore placental function over gestation., Magnetic Resonance in Medicine. 81 (2019) 1191–1204. https://doi.org/10.1002/mrm.27447.

[14] M.C. Schabel, V.H.J. Roberts, J.O. Lo, S. Platt, K.A. Grant, A.E. Frias, C.D. Kroenke, Functional imaging of the nonhuman primate Placenta with endogenous blood oxygen level–dependent contrast, Magnetic Resonance in Medicine. 76 (2016) 1551–1562. https://doi.org/10.1002/mrm.26052.

[15] M. Sinding, D.A. Peters, S.S. Poulsen, J.B. Frøkjær, O.B. Christiansen, A. Petersen, N. Uldbjerg, A. Sørensen, Placental baseline conditions modulate the

496 hyperoxic BOLD-MRI response., Placenta. 61 (2018) 17–23.
497 https://doi.org/10.1016/j.placenta.2017.11.002.
498 [16]C. Wright, D.M. Morris, P.N. Baker, I.P. Crocker, P.A. Gowland, G.J. Parker, C.P.
499 Sibley, Magnetic resonance imaging relaxation time measurements of the
500 placenta at 1.5T, Placenta. 32 (2011) 1010–1015.
501 https://doi.org/10.1016/j.placenta.2011.07.008.
502 [17]I. Huen, D.M. Morris, C. Wright, G.J.M. Parker, C.P. Sibley, E.D. Johnstone, J.H.
503 Naish, R 1 and R 2 * changes in the human placenta in response to maternal
504 oxygen challenge, Magnetic Resonance in Medicine. 70 (2013) 1427–1433.
505 https://doi.org/10.1002/mrm.24581.
506 [18]A. Sørensen, D. Peters, C. Simonsen, M. Pedersen, B. Stausbøl-Grøn, O.B.
507 Christiansen, G. Lingman, N. Uldbjerg, Changes in human fetal oxygenation
508 during maternal hyperoxia as estimated by BOLD MRI., Prenatal Diagnosis. 33
509 (2013) 141–5. https://doi.org/10.1002/pd.4025.
510 [19]E. Ingram, D. Morris, J. Naish, J. Myers, E. Johnstone, MR imaging measurements
511 of altered placental oxygenation in pregnancies complicated by fetal growth
512 restriction, Radiology. 285 (2017) 953–960.
513 https://doi.org/10.1148/radiol.2017162385.
514 [20]G.E. Chalouhi, M. Alison, B. Deloison, R. Thiam, G. Autret, D. Balvay, C.A.
515 Cuenod, O. Clément, L.J. Salomon, N. Siauve, Fetoplacental Oxygenation in an
516 Intrauterine Growth Restriction Rat Model by Using Blood Oxygen Level–
517 Dependent MR Imaging at 4.7 T, Radiology. 269 (2013) 122–129.
518 https://doi.org/10.1148/radiol.13121742.
519 [21]E. Girsh, V. Plaks, A.A. Gilad, N. Nevo, E. Schechtman, M. Neeman, N. Dekel,
520 Cloprostenol, a Prostaglandin F(2alpha) Analog, Induces Hypoxia in Rat
521 Placenta: BOLD Contrast MRI, NMR in Biomedicine. 20 (2007) 304–325.
522 https://doi.org/10.1002/nbm.
523 [22]A.E.P. Ho, J. Hutter, L.H. Jackson, P.T. Seed, L. Mccabe, M. Al-adnani, A.
524 Marnerides, S. George, L. Story, J. V Hajnal, M.A. Rutherford, L.C. Chappell, T2 *
525 Placental Magnetic Resonance Imaging An Observational Cohort Study,
526 Hypertension (Dallas, Tex. : 1979). (2020) 1–9.
527 https://doi.org/10.1161/HYPERTENSIONAHA.120.14701.
528 [23]A.J. Hirsch, V.H.J. Roberts, P.L. Grigsby, N. Haese, M.C. Schabel, X. Wang, J.O.
529 Lo, Z. Liu, C.D. Kroenke, J.L. Smith, M. Kelleher, R. Broeckel, C.N. Kreklywich,
530 C.J. Parkins, M. Denton, P. Smith, V. DeFilippis, W. Messer, J.A. Nelson, J.D.

Hennebold, M. Grafe, L. Colgin, A. Lewis, R. Ducore, T. Swanson, A.W. Legasse, M.K. Axthelm, R. MacAllister, A.V. Moses, T.K. Morgan, A.E. Frias, D.N. Streblow, Zika virus infection in pregnant rhesus macaques causes placental dysfunction and immunopathology, Nature Communications. 9 (2018) 263. https://doi.org/10.1038/s41467-017-02499-9.

[24] J.O. Lo, V.H.J. Roberts, M.C. Schabel, X. Wang, T.K. Morgan, Z. Liu, C. Studholme, C.D. Kroenke, A.E. Frias, Novel Detection of Placental Insufficiency by Magnetic Resonance Imaging in the Nonhuman Primate:, Reproductive Sciences. (2017). https://doi.org/10.1177/1933719117699704.

[25] J. Villar, L. Cheikh Ismail, C.G. Victora, E.O. Ohuma, E. Bertino, D.G. Altman, A. Lambert, A.T. Papageorghiou, M. Carvalho, Y.A. Jaffer, M.G. Gravett, M. Purwar, I.O. Frederick, A.J. Noble, R. Pang, F.C. Barros, C. Chumlea, Z.A. Bhutta, S.H. Kennedy, International Fetal and Newborn Growth Consortium for the 21st Century (INTERGROWTH-21st), International standards for newborn weight, length, and head circumference by gestational age and sex: the Newborn Cross-Sectional Study of the INTERGROWTH-21st Project., Lancet (London, England). 384 (2014) 857–68. https://doi.org/10.1016/S0140-6736(14)60932-6.

[26] P.A. Yushkevich, J. Piven, H.C. Hazlett, R.G. Smith, S. Ho, J.C. Gee, G. Gerig, User-guided 3D active contour segmentation of anatomical structures: significantly improved efficiency and reliability., NeuroImage. 31 (2006) 1116–28. https://doi.org/10.1016/j.neuroimage.2006.01.015.

[27] K.H. Zou, S.K. Warfield, A. Bharatha, C.M.C. Tempany, M.R. Kaus, S.J. Haker, W.M. Wells, F.A. Jolesz, R. Kikinis, Statistical Validation of Image Segmentation Quality Based on a Spatial Overlap Index, Acad Radiol. 11 (2004) 178–189. https://doi.org/10.1016/S1076-6332(03)00671-8.

[28] J. Hutter, L. Jackson, A. Ho, M. Pietsch, L. Story, L.C. Chappell, J. V. Hajnal, M. Rutherford, T2* relaxometry to characterize normal placental development over gestation in-vivo at 3T, Wellcome Open Research. 4 (2019) 166. https://doi.org/10.12688/wellcomeopenres.15451.1.

[29] A.R. Backes, A new approach to estimate lacunarity of texture images, Pattern Recognition Letters. 34 (2013) 1455–1461. https://doi.org/10.1016/j.patrec.2013.05.008.

[30] F. Pedregosa, G. Varoquaux, A. Gramfort, V. Michel, B. Thirion, O. Grisel, M. Blondel, A. Müller, J. Nothman, G. Louppe, P. Prettenhofer, R. Weiss, V. Dubourg, J. Vanderplas, A. Passos, D. Cournapeau, M. Brucher, M. Perrot, É.

566 Duchesnay, Scikit-learn: Machine Learning in Python, Journal of Machine
567 Learning Research. 12 (2012) 2825–2830.
568 [31]A.F. Marquand, I. Rezek, J. Buitelaar, C.F. Beckmann, Understanding
569 Heterogeneity in Clinical Cohorts Using Normative Models: Beyond Case-Control
570 Studies, Biological Psychiatry. 80 (2016) 552–561.
571 https://doi.org/10.1016/j.biopsych.2015.12.023.
572 [32]I.M. Beune, F.H. Bloomfield, W. Ganzevoort, N.D. Embleton, P.J. Rozance, A.G.
573 van Wassenaer-Leemhuis, K. Wynia, S.J. Gordijn, Consensus Based Definition of
574 Growth Restriction in the Newborn, J Pediatr. 196 (2018) 71-76.e1.
575 https://doi.org/10.1016/j.jpeds.2017.12.059.
576 [33]G. Mielke, N. Benda, Cardiac output and central distribution of blood flow in the
577 human fetus., Circulation. 103 (2001) 1662–8.
578 https://doi.org/10.1161/01.cir.103.12.1662.
579 [34]M. Seed, J. F P van Amerom, S.-J. Yoo, B. Nafisi, L. Grosse-Wortmann, E. Jaeggi,
580 M.S. Jansz, C.K. Macgowan, Feasibility of quantification of the distribution of
581 blood flow in the normal human fetal circulation using CMR: a cross-sectional
582 study, Journal of Cardiovascular Magnetic Resonance. 14 (2012) 79.
583 https://doi.org/10.1186/1532-429X-14-79.
584 [35]N.B. Matthiesen, T.B. Henriksen, P. Agergaard, J.W. Gaynor, C.C. Bach, V.E.
585 Hjortdal, J.R. Østergaard, Congenital Heart Defects and Indices of Placental and
586 Fetal Growth in a Nationwide Study of 924 422 Liveborn Infants, Circulation. 134
587 (2016) 1546–1556. https://doi.org/10.1161/CIRCULATIONAHA.116.021793.
588 [36]E. Llurba, O. Sánchez, Q. Ferrer, K.H. Nicolaides, A. Ruíz, C. Domínguez, J.
589 Sánchez-de-Toledo, B. García-García, G. Soro, S. Arévalo, M. Goya, A. Suy, S.
590 Pérez-Hoyos, J. Alijotas-Reig, E. Carreras, L. Cabero, Maternal and foetal
591 angiogenic imbalance in congenital heart defects, European Heart Journal. 35
592 (2014) 701–707. https://doi.org/10.1093/eurheartj/eht389.
593 [37]C.E.G. Head, V.C. Jowett, G.K. Sharland, J.M. Simpson, Timing of presentation
594 and postnatal outcome of infants suspected of having coarctation of the aorta
595 during fetal life, Heart. 91 (2005) 1070–1074.
596 https://doi.org/10.1136/hrt.2003.033027.
597 [38]J.O. Miranda, L. Hunter, S. Tibby, G. Sharland, O. Miller, J.M. Simpson, Myocardial
598 deformation in fetuses with coarctation of the aorta: a case-control study,
599 Ultrasound Obstet Gynecol. 49 (2017) 623–629.
600 https://doi.org/10.1002/uog.15939.

[39]W. You, N.N. Andescavage, K. Kapse, M.T. Donofrio, M. Jacobs, C. Limperopoulos, Hemodynamic Responses of the Placenta and Brain to Maternal Hyperoxia in Fetuses with Congenital Heart Disease by Using Blood Oxygen-Level Dependent MRI., Radiology. (2019) 190751. https://doi.org/10.1148/radiol.2019190751.

[40]J. Co-Vu, D. Lopez-Colon, H.V. Vyas, N. Weiner, C. DeGroff, Maternal hyperoxygenation: A potential therapy for congenital heart disease in the fetuses? A systematic review of the current literature, Echocardiography. 34 (2017) 1822–1833. https://doi.org/10.1111/echo.13722.

[41]Q.N. Do, M.A. Lewis, A.J. Madhuranthakam, Y. Xi, A.A. Bailey, R.E. Lenkinski, D.M. Twickler, Texture analysis of magnetic resonance images of the human placenta throughout gestation: A feasibility study, PLOS ONE. 14 (2019) e0211060. https://doi.org/10.1371/journal.pone.0211060.

[42]N. Andescavage, S. Dahdouh, M. Jacobs, S. Yewale, D. Bulas, S. Iqbal, A. Baschat, C. Limperopoulos, In vivo textural and morphometric analysis of placental development in healthy & growth-restricted pregnancies using magnetic resonance imaging, Pediatric Research. 85 (2019) 974–981. https://doi.org/10.1038/s41390-019-0311-1.

[43]A.M. El-Ali, W. Reynolds, V. Rajagopalan, V. Lee, J. Wallace, J. Schabdach, A. Zehner, M. Gruss, J.H. Adibi, V. Schmithorst, A. Panigrahy, BOLD MR Imaging of Placenta in Congenital Heart Disease: Correlation with Maternal Risk Factors, Placental Pathology, and Maternal Serum Hormones [abstract], ISMRM 27th Annual Meeting & Exhibition. (2019). https://doi.org/10.1101/388074.

[44]E.A. Turk, S.M. Abulnaga, J. Luo, J.N. Stout, H.A. Feldman, A. Turk, B. Gagoski, L.L. Wald, E. Adalsteinsson, D.J. Roberts, C. Bibbo, J.N. Robinson, P. Golland, P.E. Grant, W.H. Barth, Placental MRI: Effect of maternal position and uterine contractions on placental BOLD MRI measurements, Placenta. (2020). https://doi.org/10.1016/j.placenta.2020.04.008.

[45]S.J. Gordijn, I.M. Beune, B. Thilaganathan, A. Papageorghiou, A.A. Baschat, P.N. Baker, R.M. Silver, K. Wynia, W. Ganzevoort, Consensus definition of fetal growth restriction: a Delphi procedure, Ultrasound in Obstetrics & Gynecology. 48 (2016) 333–339. https://doi.org/10.1002/uog.15884.

[46]N.B. Matthiesen, T.B. Henriksen, J.W. Gaynor, P. Agergaard, C.C. Bach, V.E. Hjortdal, J.R. Østergaard, Congenital Heart Defects and Indices of Fetal Cerebral

635 Growth in a Nationwide Cohort of 924 422 Liveborn Infants., Circulation. 133
636 (2016) 566–75. https://doi.org/10.1161/CIRCULATIONAHA.115.019089.
637 [47]R. Avni, O. Golani, A. Akselrod-Ballin, Y. Cohen, I. Biton, J.R. Garbow, M.
638 Neeman, MR Imaging–derived Oxygen-Hemoglobin Dissociation Curves and
639 Fetal-Placental Oxygen-Hemoglobin Affinities, Radiology. 280 (2016) 68–77.
640 https://doi.org/10.1148/radiol.2015150721.
641 [48]L. Sun, D. Marini, B. Saini, E. Schrauben, C.K. Macgowan, M. Seed,
642 Understanding Fetal Hemodynamics Using Cardiovascular Magnetic Resonance
643 Imaging, FDT. 47 (2020) 354–362. https://doi.org/10.1159/000505091.
644 [49]J. Hutter, A.A. Harteveld, L.H. Jackson, S. Franklin, C. Bos, M.J.P. Osch, J.
645 O'Muircheartaigh, A. Ho, L. Chappell, J. V. Hajnal, M. Rutherford, E. De Vita,
646 Perfusion and apparent oxygenation in the human placenta (PERFOX), Magnetic
647 Resonance in Medicine. 83 (2020) 549–560. https://doi.org/10.1002/mrm.27950.
648 [50]A. Melbourne, R. Aughwane, M. Sokolska, D. Owen, G. Kendall, D. Flouri, A.
649 Bainbridge, D. Atkinson, J. Deprest, T. Vercauteren, A. David, S. Ourselin,
650 Separating fetal and maternal placenta circulations using multiparametric MRI,
651 Magnetic Resonance in Medicine. 81 (2019) 350–361.
652 https://doi.org/10.1002/mrm.27406.
653 [51]N.S. Dellschaft, G. Hutchinson, S. Shah, N.W. Jones, C. Bradley, L. Leach, C.
654 Platt, R. Bowtell, P.A. Gowland, The haemodynamics of the human placenta in
655 utero, PLOS Biology. 18 (2020) e3000676.
656 https://doi.org/10.1371/journal.pbio.3000676.
657 [52]P.J. Slator, J. Hutter, L. McCabe, A.D.S. Gomes, A.N. Price, E. Panagiotaki, M.A.
658 Rutherford, J.V. Hajnal, D.C. Alexander, Placenta microstructure and
659 microcirculation imaging with diffusion MRI, Magnetic Resonance in Medicine. 80
660 (2018) 756–766. https://doi.org/10.1002/mrm.27036.
661 [53]Z. Zun, G. Zaharchuk, N.N. Andescavage, M.T. Donofrio, C. Limperopoulos, Non-
662 Invasive Placental Perfusion Imaging in Pregnancies Complicated by Fetal Heart
663 Disease Using Velocity-Selective Arterial Spin Labeled MRI., Scientific Reports. 7
664 (2017) 16126. https://doi.org/10.1038/s41598-017-16461-8.
665 [54]Z. Zun, C. Limperopoulos, Placental perfusion imaging using velocity-selective
666 arterial spin labeling, Magn Reson Med. 80 (2018) 1036–1047.
667 https://doi.org/10.1002/mrm.27100.
668

Tables/figures

	Median	IQR	Min	Max	p
Control cohort (n=37)					
Maternal age at scan (a)	34.65	4.65	27.69	44.03	
Maternal BMI at scan (kg/m^2)	30.03	8.67	18.75	42.59	
Gestational age at scan (w)	30.86	8.36	19.57	37.86	
Fetal sex (female/total)	0.62				
Gestational age at birth (w)	40.14	2.14	38.14	42.14	
Birth weight (g)	3583	534	2780	4450	
BW Z-score	0.9558	1.2147	-1.0550	2.1966	
BW Centile	83.04	39.16	14.57	98.60	
CHD cohort (n=69)					
Maternal age at scan (a)	32.63	8.39	18.60	40.79	0.002†
Maternal BMI at scan (kg/m^2)	28.39	5.63	18.81	40.35	0.094†
Gestational age at scan (w)	31.57	2.64	28.43	36.29	0.069†
Fetal sex (female/total)	0.58				0.836
Gestational age at birth (w)	38.71	1.57	32.71	41.71	<0.001
Birth weight (g)	3080	964	1610	5150	<0.001
BW Z-score	-0.1230	1.7762	-2.9547	3.7986	0.003
BW Centile	48.20	62.20	0.16	99.99	0.003
Diagnosis	N	%			
Left-sided obstructive lesions	10	14.5	HLHS		
	13	18.8	COA- (suspected, not confirmed)		
	8	11.6	COA+ (confirmed neonatal)		
Right-sided obstructive lesions	10	14.5	TOF, PA, PS, TA, Ebstein anomaly		
Disorders of mixing	5	7.2	TGA		
Suspected vascular rings	17	24.6	DAA, RAA (+/- ALSA)		
Other major lesions	6	8.7	CAT, PAPVD, CR		

Table 1: Maternal and pregnancy characteristics.

(†) For statistical analysis controls were restrained to GA range at scan (28 – 37 weeks, N=23).

Mean deviation from GP [Z-score] +/- SD of Z-scores within group									
	Control	CHD	HLHS	COA-	COA+	RSOL	TGA	Other	VR
N	9	69	10	13	8	10	5	6	17
Mean T2*	-0.56 +/-1.34	0.93* +/-2.26	0.64 +/-2.03	1.39* +/-2.91	0.24 +/-1.34	2.30*** +/-2.07	-0.11 +/-1.86	2.31** +/-2.01	0.09 +/-2.06
Skewness	-0.08 +/-0.59	-1.99* +/-4.27	-1.12 +/-1.58	-3.83 +/-7.18	-0.66 +/-0.73	-4.69* +/-5.56	0.02 +/-0.73	-1.75** +/-1.25	-0.80 +/-2.70
Kurtosis	-0.53 +/-1.01	-1.67 +/-2.34	-0.98 +/-1.39	-2.86* +/-3.25	-0.98 +/-0.67	-3.47** +/-3.02	-0.27 +/-1.50	-1.97** +/-0.93	-0.73 +/-1.66
Lacunarity	-0.15 +/-1.27	-0.54 +/-1.55	-0.18 +/-1.21	-1.02 +/-1.69	0.26 +/-0.53	-1.70* +/-1.99	-0.01 +/-0.98	-1.26 +/-2.35	0.06 +/-0.93
Median deviation from GP [Z-score] (IQR within group)									
	Control	CHD	HLHS	COA-	COA+	RSOL	TGA	Other	VR
N	9	69	10	13	8	10	5	6	17
Mean T2*	-0.78 (2.05)	0.70* (2.93)	0.57 (2.37)	0.89* (4.05)	0.25 (2.06)	2.36*** (3.32)	-0.41 (3.68)	2.10** (3.77)	-0.59 (2.76)
Skewness	0.01 (0.71)	-0.47* (2.19)	-0.49 (2.94)	-0.96 (4.38)	-0.62 (0.98)	-2.12* (10.23)	0.73 (2.32)	-1.89** (2.40)	0.02 (0.83)
Kurtosis	-0.80 (1.67)	-1.10 (1.95)	-0.75 (2.07)	-1.72* (3.35)	-0.86 (1.04)	-2.15** (5.64)	0.41 (2.65)	-1.83** (1.83)	-0.63 (1.23)
Lacunarity	0.01 (1.95)	-0.18 (1.67)	-0.09 (1.28)	-0.68 (2.49)	0.17 (0.82)	-1.43* (2.22)	0.29 (1.84)	-0.37 (3.84)	0.05 (1.35)

Table 2: Results Gaussian process Regression, groupwise.

Entire CHD cohort (CHD), Hypoplastic left heart syndrome (HLHS), Coarctation suspected not confirmed (CoA-), Coarctation confirmed operated (CoA+), Right-sided obstructive lesions (RSOL), Disorders of mixing (TGA), Other lesions, Suspected vascular rings (VR). Significance calculated by Independent t-test (Mean T2*) or Mann-Whitney U (Skewness, Kurtosis, Lacunarity) in comparison to test control cohort, * $p \leq 0.05$, ** $p \leq 0.01$, *** $p \leq 0.001$.

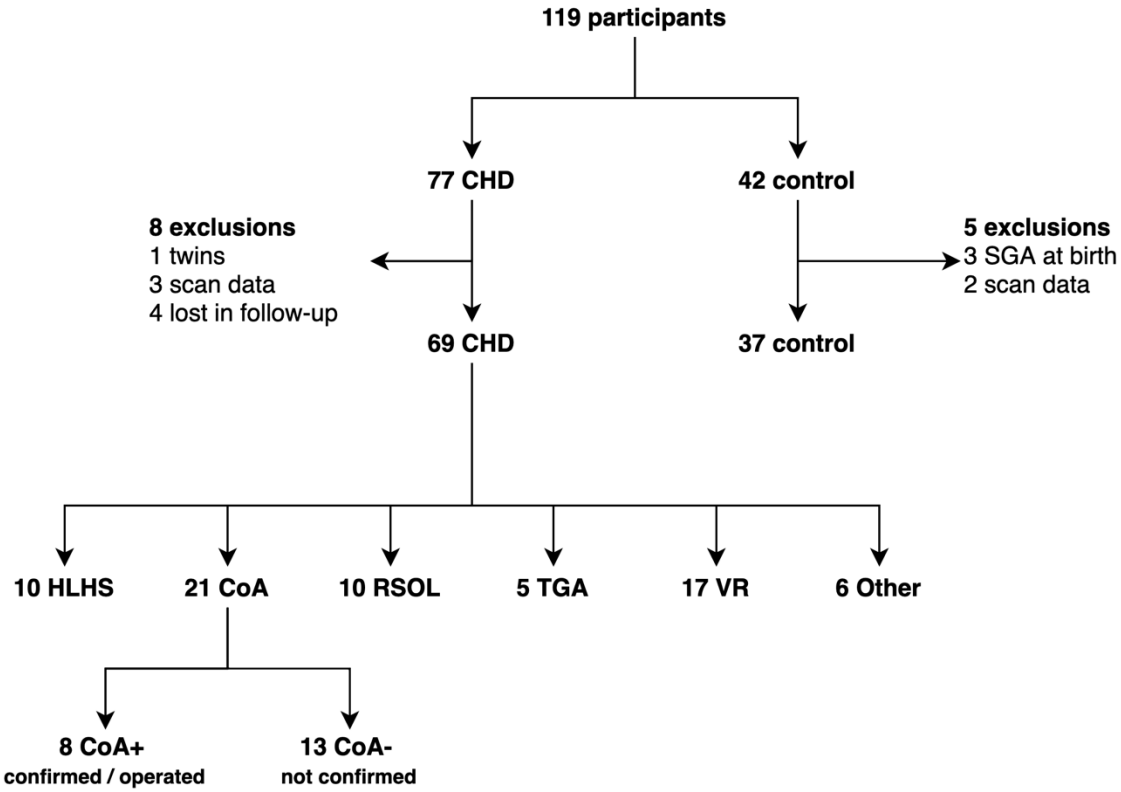

Figure 1 - Study cohort.

CHD subtypes classified by main antenatal diagnosis: Hypoplastic left heart (HLHS), coarctation of the aorta (CoA), right-sided obstructive lesions (RSOL), transposition of the great arteries (TGA), suspected vascular ring (VR) and other complex lesions. Controls were excluded for low birth weight (SGA) and insufficient scan data, pregnancies complicated by fetal CHD had to be excluded for twin pregnancy and loss in follow-up at time of analysis.

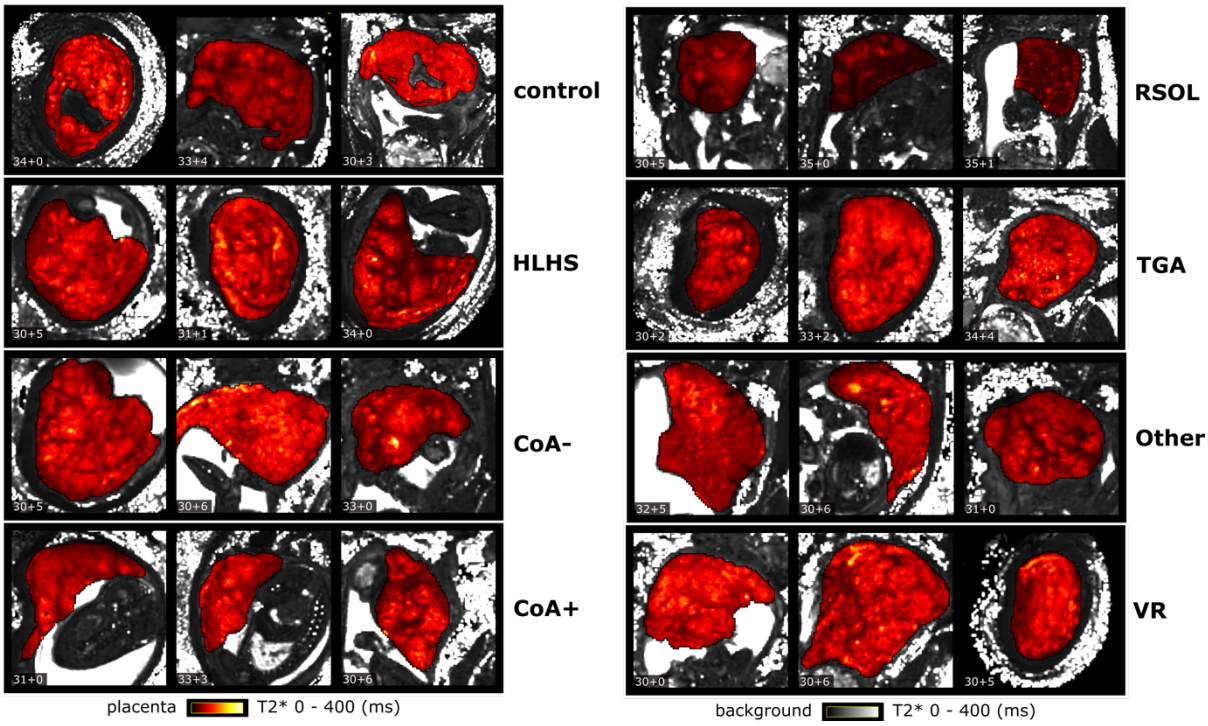

Figure 2: Qualitative Imaging

Illustration of mid-stack slice in coronal orientation from T2* maps from 3 individual placentas for all included cohorts. Segmented placental parenchyma is highlighted in red/yellow scales.

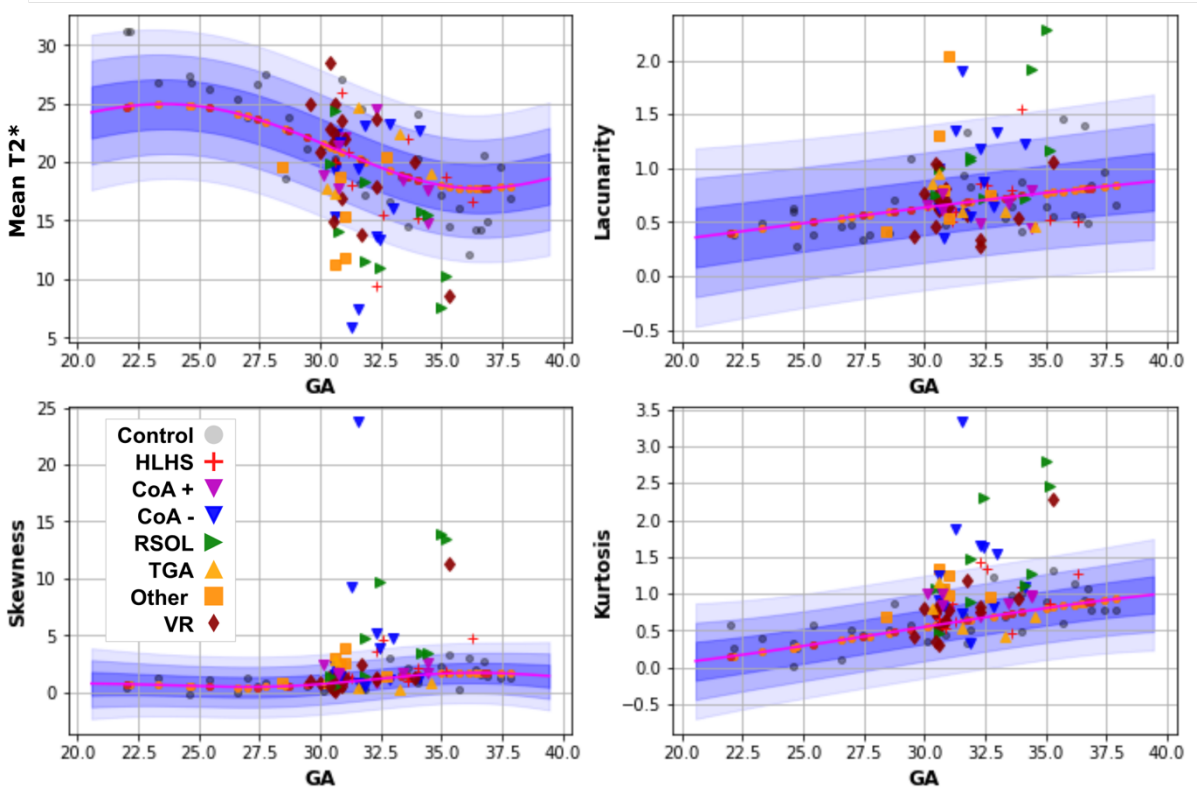

Figure 3 – Gaussian Process Regression results

The posterior probability for Mean T2*, Lacunarity, Skewness and Kurtosis over GA for all considered controls in red, the corridors corresponding to Z-scores of 1, 2 and 3 are illustrated in blue. Cohorts: Control (test subset), Hypoplastic left heart syndrome (HLHS), Coarctation of the aorta confirmed (COA+) and not confirmed (COA-), right-sided obstructive lesions (RSOL), disorders of mixing (TGA), other major lesions and suspected vascular rings (VR).

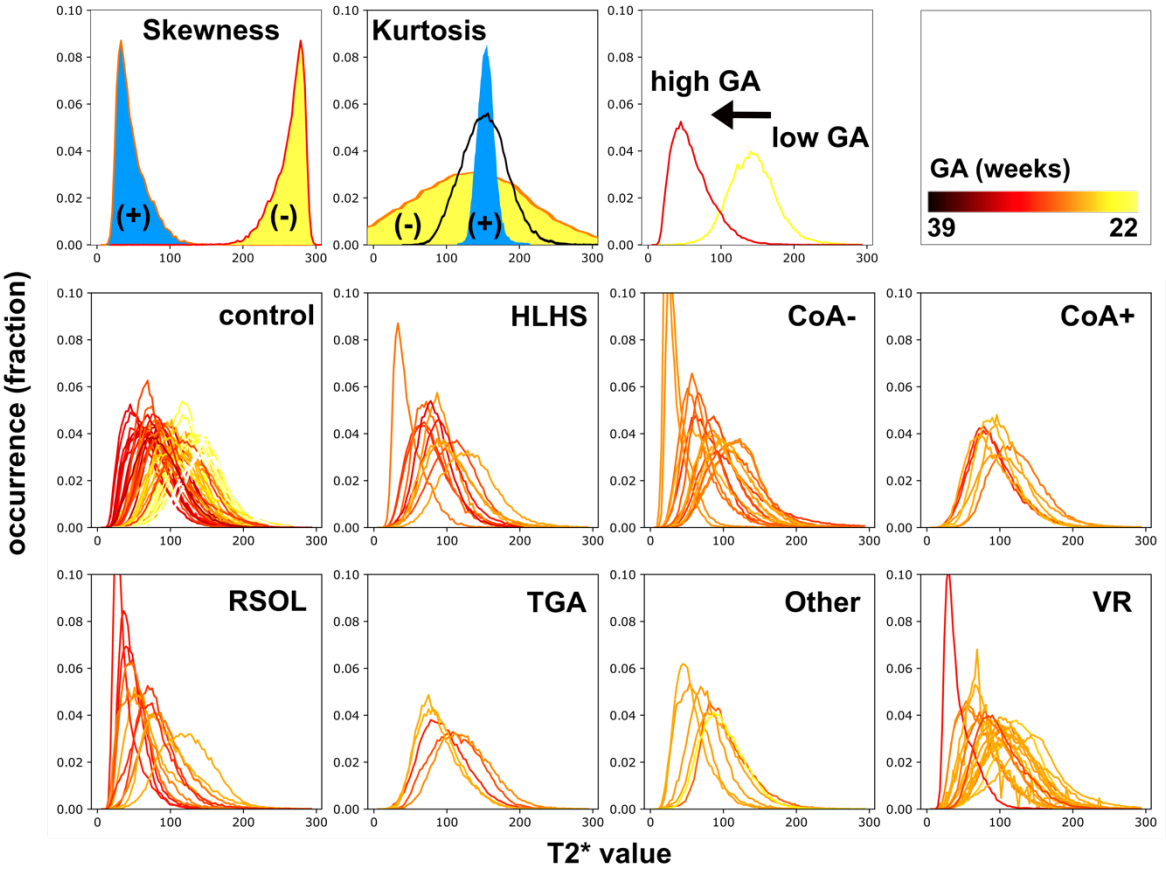

Figure 4 - Individual Histograms

Individual Histograms, derived from about 70000 voxels per subject binned in 100, depicting occurrence fraction of T2* values over the entire placental volume from all participants, coloured by GA at scan. Groups from top left to bottom right. Control, Hypoplastic left heart syndrome (HLHS), coarctation of the aorta not confirmed (CoA-) and confirmed (COA+), right-sided obstructive lesion (RSOL), Transposition of the great arteries (TGA), Other lesions and suspected vascular ring (VR).

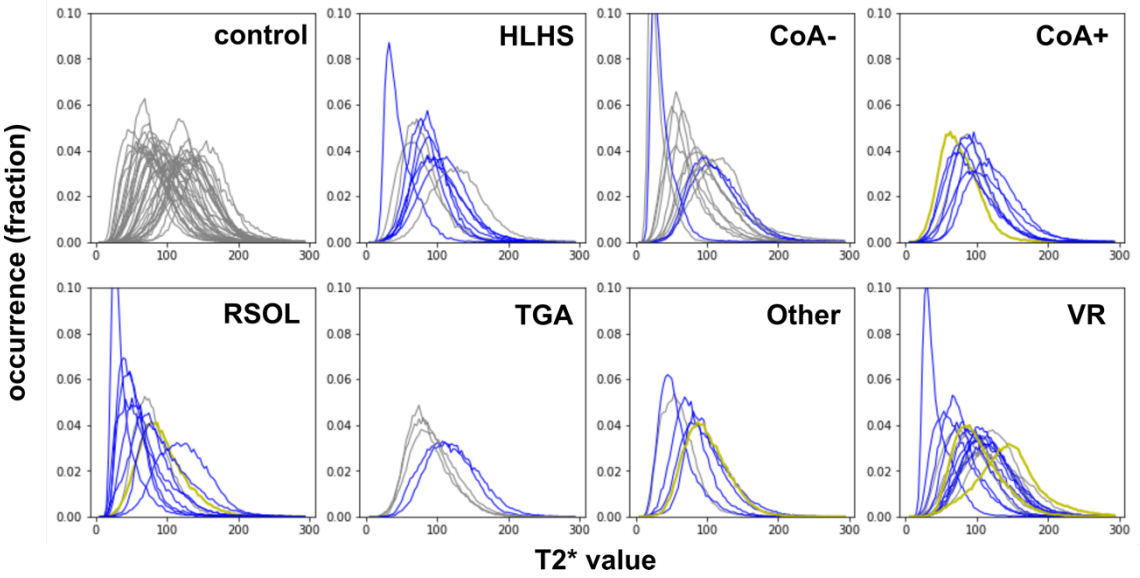

Supplemental Figure 1 – Histograms with genetic test results

Individual Histograms, as shown in Figure 4. Color coded by results of genetic testing. Abnormal genetics (yellow), normal genetics (blue), not tested (grey), Hypoplastic left heart syndrome (HLHS), coarctation of the aorta not confirmed (CoA-) and confirmed (COA+), right-sided obstructive lesion (RSOL), Transposition of the great arteries (TGA), Other lesions and suspected vascular ring (VR).

N (%)	Control	CHD
Available placental histology	15/37 (40%)	12/69 (17%)
MVM	1	2
With infarct	1	2
(Sub-)Chorionitis	8	7
With MIR	4	3
With FIR	5	4

Supplemental Table 1 – Placental Histology

Table shows available placental histology results. Maternal vascular malperfusion (MVM), maternal inflammatory response (MIR), fetal inflammatory response (FIR).

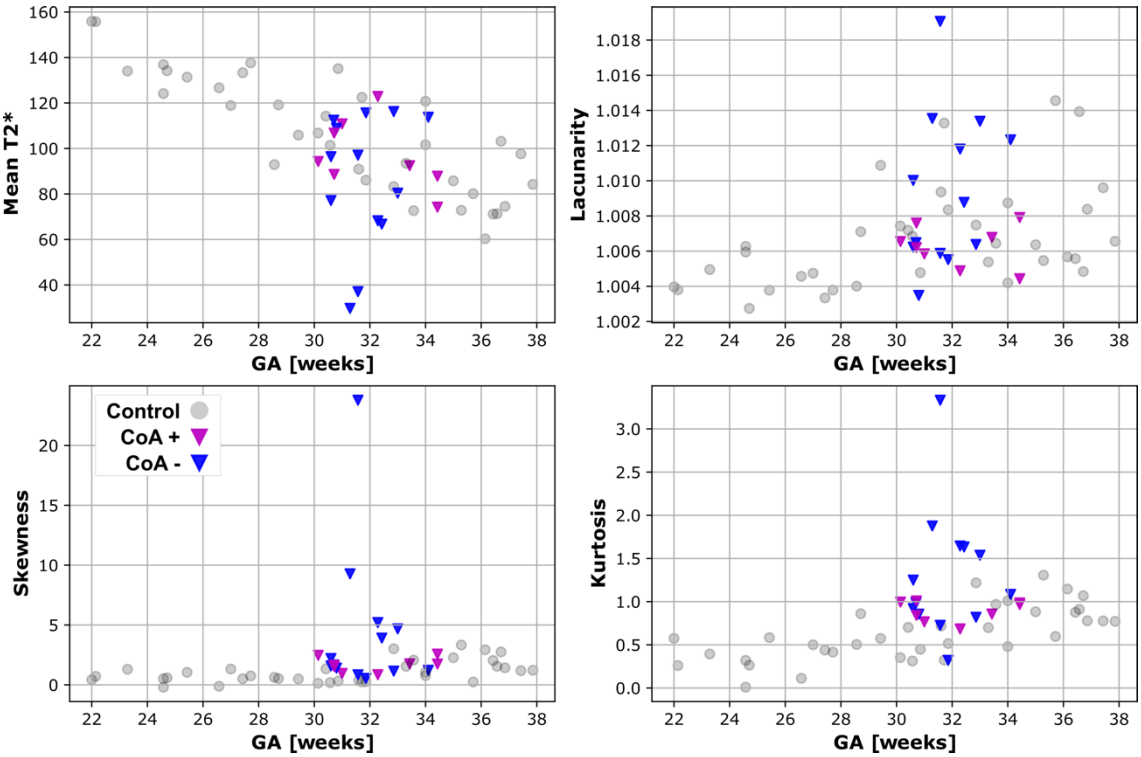

Supplemental Figure 2 – Coarctation of the aorta cohort and controls

Mean T2*, Lacunarity, Skewness and Kurtosis over GA for all included controls in grey, confirmed Coarctation of the aorta (CoA+) in pink and not confirmed (CoA-) in blue.